JGR Oceans

RESEARCH ARTICLE
10.1029/2022JC019257

Variability of the Shelf Circulation Around South Georgia, Southern Ocean

V. Combes[1,2,3], R. P. Matano[3], M. P. Meredith[4], and E. F. Young[4]

[1]Institut Mediterrani d'Estudis Avançats (IMEDEA) (CSIC-UIB), Esporles, Spain, [2]Departament de Física, Universitat de les Illes Balears, Palma de Mallorca, Spain, [3]College of Earth, Ocean and Atmospheric Sciences, Oregon State University, Corvallis, OR, USA, [4]British Antarctic Survey, Cambridge, UK

Key Points:

- The shelf circulation of South Georgia exhibits strong interannual variability
- The local wind stress and the south ACC front are the main drivers of variability of both shelf circulation and cross-shelf mass exchanges
- El Niño Southern Oscillation does not significantly contribute to the shelf circulation but is significantly correlated with the surface temperature variability

Supporting Information:

Supporting Information may be found in the online version of this article.

Correspondence to:

V. Combes,
vcombes@imedea.uib-csic.es

Citation:

Combes, V., Matano, R. P., Meredith, M. P., & Young, E. F. (2023). Variability of the shelf circulation around South Georgia, Southern Ocean. *Journal of Geophysical Research: Oceans*, *128*, e2022JC019257. https://doi.org/10.1029/2022JC019257

Received 4 SEP 2022
Accepted 25 JAN 2023

Abstract A high-resolution ocean model is used to characterize the variability of the shelf circulation and cross-shelf transport around the South Georgia island (SG). The time-mean shelf circulation consists of a counterclockwise flow with a net onshelf mass flow in the south and a net offshelf mass flow in the north. In the south, the cross-shelf exchanges show a two-layer structure with an offshelf flow below 350 m and onshelf flow above. In the north, the cross-shelf exchanges show a three-layer structure with the onshelf flow found only between 350 and 50 m. Correlation analysis shows that winds and the Southern Antarctic Circumpolar Current Front (SACCF) current modulate the variability of the shelf circulation and cross-shelf transport. Local wind stress is significantly correlated with the coastal currents, mid-shelf jet, and cross-shelf transports in the upper layer, while the SACCF modulates the shelf and cross-shelf transports in the southwestern shelf. Likewise, an Empirical Orthogonal Function analysis indicates that the first mode of shelf circulation variability is highly correlated with the SACCF, while the second mode is explained by the local wind stress and significantly correlated with the Antarctic Oscillation. The El Niño Southern Oscillation does not significantly contribute to the shelf circulation but is significantly correlated with the surface temperature variability. The atmospheric teleconnection drives changes in local heat flux, such that warm El Niño conditions over the equatorial Pacific are associated with a cooling of the SG waters. This superposes local signals onto temperature anomalies advected from upstream in the ACC found in previous studies.

Plain Language Summary Over the last decades, the Southern Ocean has undergone strong interannual variability. Here, we focus on the region around the island of South Georgia, where intense blooms of phytoplankton were recorded by in situ and remote satellite data. We use a high-resolution ocean model to describe the variability of the circulation around the island and of the flow of the nutrient-rich shelf waters into the open ocean. We find that the local wind stress and the nearby ocean large-scale current, known as the Southern Antarctic Circumpolar Current Front, are the main drivers of the shelf circulation variability. We also find that the variability of the shelf water temperature is linked to the variability observed in the equatorial Pacific (El Niño Southern Oscillation).

1. Introduction

South Georgia (SG) is a small (~170 × 35 km) Southern Ocean island bounded by the swift flow of the Southern Antarctic Circumpolar Current Front (SACCF). Despite its diminutive size, SG is a region of great oceanographic interest due to the high fertility of its waters, which sustain a rich marine ecosystem that extends well beyond its shelf region. The most obvious manifestations of SG's fertility are its exceptional chlorophyll blooms—one of the Southern Ocean largest—which evidence an active fertilization process mediated by local atmospheric forcing, shelf/open ocean exchanges and glacial discharges (Fielding et al., 2014; Meredith et al., 2003, 2005; Young et al., 2014). Studies dating back to the beginning of the last century have described the oceanic circulation patterns around SG, and their potential links to the fertility of the coastal waters (Hardy & Gunther, 1935; Hart, 1934). Several of these studies also discuss the links between variations of physical properties within the SG shelf and changes of the large scale oceanic and atmospheric circulations (Deacon, 1977; Maslennikov & Solyankin, 1981; Meredith et al., 2005; Thorpe et al., 2002; Whitehouse et al., 1996).

Sea Surface Temperature (SST) variability is one of the best documented low-frequency, shelf/large scale connections. Trathan and Murphy (2003), for example, showed significant correlations between SST variability around SG and the El Niño Southern Oscillation (ENSO) phenomenon, with advective time lags of approximately 3 years.

Meredith et al. (2005, 2008) added that SST anomalies around SG can also be influenced by ENSO and Antarctic Oscillation index (AAO) on significantly shorter time scales (order of months). There are, however, significantly fewer studies on the links between open ocean/shelf circulation variability, most of which have been focused on the influence of the SACCF position on the physical properties over the shelf (Meredith et al., 2005; Thorpe et al., 2002, 2004; Trathan et al., 1997, 2000; Young et al., 2014) or on the SG ecosystem (Trathan et al., 2003).

In a prior article Matano et al. (2020, M20 hereafter) we used the results of a high-resolution ocean model to characterize the time mean circulation over the SG shelf and to investigate the dynamical processes mediating the water exchanges between the shelf and the open ocean. We showed that the SACCF pumps iron-enriched waters from the deep ocean onto the bottom layers of South Georgia's shelf. These waters are upwelled along the northern coast of the island and are then exported into the Georgia Basin, where topographically steered circulation shields them from the dispersive effects of local currents and eddies, thus allowing the bloom development. This article expands the results described by M20. Here we use similar model results to characterize the dominant modes of low-frequency variability (seasonal and interannual) of SG's shelf circulation and identify their dynamical drivers. To the best of our understanding there are no prior studies on the low-frequency variability of SG's shelf circulation.

2. Model and Data Description

The model configuration used in this study is described in detail in M20 but for the sake of completeness a brief description is included here. We use the Adaptative Mesh Refinement In Fortran (AGRIF) version of the Regional Ocean Modeling System (ROMS, Debreu et al., 2011; Shchepetkin & McWilliams, 2005). This is a three-dimensional, free surface, hydrostatic, eddy-resolving primitive equation ocean model using sigma coordinates in the vertical. The model grid extends from 45.7°W to 30.7°W and from 58°S to 48°S (Figure S1 in Supporting Information S1). It has a spatial resolution of 1/36° (∼2 km) and 40 terrain-following levels in the vertical. At the lateral boundaries, the model is nudged toward the 5-day averaged output from the model used in M20. The latter experiment also provides the initial conditions. At the surface, the model is forced by the daily averaged relative humidity, precipitation, long/shortwave radiation, 10 wind, and 2 m air temperature fields from the ERA5 data set (Hersbach et al., 2018). To assess the quality of the ERA5 wind in this region we compared it with wind data from QSCAT(2000–2008)/ASCAT(2009–2016) satellite scatterometers. An Empirical Orthogonal Function (EOF) analysis shows that the first and second modes of the model wind stress variability (derived from ERA5 10 m winds) are highly correlated with those from QSCAT/ASCAT scatterometers (Figure S2 in Supporting Information S1). The model also includes the monthly climatology discharge of 51 glaciers (Young et al., 2011) and the eight principal tidal components (M2, S2, N2, K2, K1, O1, P1, and Q1 from the TPXO9 atlas, Egbert & Erofeeva, 2002). This configuration was run for the period 1994–2016 and the output was averaged every 5 days.

Observed sea surface temperatures (SST) are obtained from the Operational SST and Sea Ice Analysis (OSTIA) data set (Good et al., 2020), which is available at http://marine.copernicus.eu. OSTIA's SSTs are produced from in situ and satellite observations and interpolated to a 0.05° grid.

To ascribe causality, the time series of the model derived modes are compared with climate indexes of Southern Ocean variability, namely the Antarctic Oscillation (AAO) and the Southern Oscillation Index (SOI). The AAO is the dominant mode of extra-tropical climate variability in the Southern Hemisphere. It is defined as the first mode of the 700 hPa height variability south of 20°S, which reflects fluctuations of zonal winds over the Southern Ocean. The AAO has moved to a more positive state (stronger, circumpolar-intensified winds) in recent decades (Cai et al., 2003; Fyfe et al., 1999; Hao et al., 2017; Shindell & Schmidt, 2004). The SOI index, derived from the sea level pressure difference between Tahiti and Darwin, characterizes Southern Ocean ENSO variability, which manifests as a Rossby wave train spanning the south Pacific with alternating nodes of high/low heat flux and SST anomaly. The SOI and SSO indices are obtained at https://www.cpc.ncep.noaa.gov/data.

In what follows the term "seasonal cycle" refers to time series reconstructed from harmonics with frequencies of 1, 2, and 3 cycles per year. The term "interannual variability" refers to the time series obtained after removing the seasonal cycle defined above. Hereafter and unless explicitly stated otherwise, all analyses are done using the interannual variability component of the time series and the term "variability" will refer to "interannual variability." All correlation coefficients above the 95% confidence level are marked with the symbol "*." We define

the shelf as the region between the coast and the 500 m isobath (Figure 1a). The term open-ocean will refer to the region outside the shelf. Alongshelf transport refers to the transport integrated from the coast to the shelfbreak and it is defined as positive in the counter-clockwise direction. Hereafter and unless explicitly stated otherwise, the wind stress time series corresponds to the zonal model wind stress at 37°W–53.5°S. Note that over the SG region (40°W–34°W/56°S–53°S), the 0.25° resolution ERA5 winds are largely homogeneous ($R > 0.85$, also inferred from the EOFs decomposition in Figure S2 in Supporting Information S1).

3. Results

3.1. Circulation

3.1.1. Time Mean Horizontal Circulation and Obduction

Circulation over the SG shelf is dominated by a counterclockwise flow, upon which is superposed small-scale vortices and meanders shaped by the bottom topography (Figure 1a). Along the southern rim of the island flows a strong coastal current (mean speeds greater than 8 cm/s), which, after reaching the southeastern corner of the island, continues as a broad mid-shelf jet with mean speed of ∼6 cm/s. Along the northern rim of the island there is another coastal current flowing eastward which is generated by the upwelling-favorable winds, as per M20. The time mean alongshelf transport—defined as the transport integrated between the coast and the shelfbreak—is of the order of 0.2 Sv although its value varies with location (M20, Figure 1b). Cross-shelf exchanges, that is, volume fluxes across the 500 m isobath, are characterized by a net onshelf mass flow south of the island and an offshelf mass flow north of it (Figure 1b). Cross-shelf exchanges in the northern and southern region have quite distinct vertical structures. The inflow in the southern region, for example, is largely constrained to the top layers with a weaker offshelf flow below 350 m (Figure 1c). The outflow in the northern region, however, has a more complex three-layer structure with outflows above 50 m and below 350 m, and an inflow between 50 and 350 m (Figure 1c). Topographic effects on cyclonic shelfbreak jets—like the portion of the SACCF flowing along the northern slope of SG—generate upwelling and a downslope flux of mass in the deep layers (Combes & Matano, 2014; Matano & Palma, 2008; Miller et al., 2011). Cross-shelf exchanges in the upper layer (0–50 m) are consistent with Ekman dynamics, with onshelf and offshelf flows in the southern and northern portions of the island, respectively (Figure 1c).

3.1.2. Drivers of Circulation

Winds and the SACCF are two of the most important drivers of the SG shelf horizontal circulation (M20). There are significant correlations between wind stress and the alongshelf transport in the western and eastern sides of SG, where variations of the wind stress magnitude are followed by proportional variations of the transport (Figure 2a). The eastward component of the wind stress is proportional to the northward transport (clockwise, $|R| = 0.44$*) west of the SG and to the northward transport (counterclockwise, $R = 0.58$*) east of the SG. There are no significant correlations between wind stress forcing and alongshelf transport in the northern and southern portions of the SG shelf. In those regions wind stress is only correlated with the transport of the coastal currents flowing along the northern and southern sides of the island ($R > 0.5$*, Figure 2b), consistent with a geostrophic adjustment of coastal currents from downwelling-favorable westerly winds in the south and upwelling-favorable westerly winds in the north. As expected, the variability of the velocities of the mid-shelf jet that originates from the southern coastal current is significantly correlated with the wind stress ($R > 0.5$*). There is also a significant correlation between the zonal wind stress and the offshelf transport north of SG ($R = 0.65$*, Figure 2c). There is no significant correlation between wind stress and the vertically integrated cross-shelf transport in the southern region. Consistent with Ekman dynamics, cross shelf exchanges in the upper layer (0–50 m) are modulated by the wind stress variability in the offshelf direction in the northern shelf ($R = 0.92$*) and in the onshelf direction in the southern shelf ($R = 0.70$*, Figure 2d).

To estimate the influence of the SACCF on the shelf circulation, we calculated the correlation between its transport (magenta transect, Figure 3a) and cross-shelf and alongshelf transports. The largest correlation is observed in the southwestern shelf (Figures 3a and 3b), which is the region where the SACCF—after encountering the shelf slope—bifurcates into two branches, one flowing toward the southeast and the other toward the northwest (Figure 3c). The west branch intrudes onto the shelf increasing the alongshelf transport. The variability of the SACCF transport is also correlated with variations of the transport in the shelf canyons (Figure 3d). There is a significant correlation between the SACCF westward transport at 37.2°W and the subsurface (100–200 m;

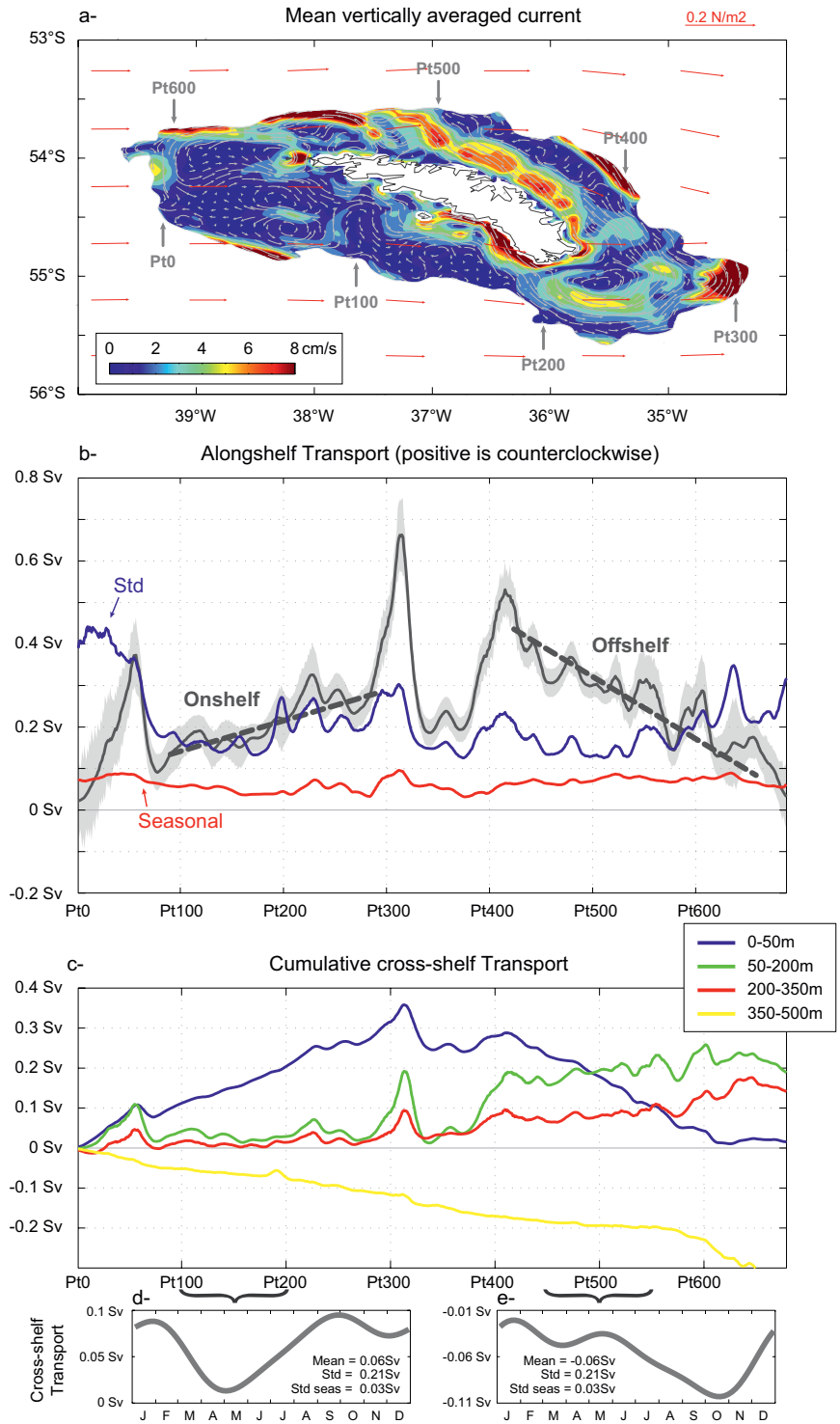

Figure 1. *Mean/Variability shelf circulation*. (a) Time-averaged vertically averaged current (gray arrows and colors) and surface wind stress (red arrows). The currents are shown only for depths shallower than 500 m ("shelf"). Pt0-Pt688 refer to the position along the shelfbreak in the counterclockwise direction used as the *x*-axis in panels (b and c). (b) Shows the mean (black), standard deviation (blue), and seasonal amplitude (red) of the alongshelf transports between 500 m and the coast. The gray area in panel (b) corresponds to the standard deviation of the yearly averaged time series. (c) Cumulative cross-shelf transport integrated between 0 and 50 (blue), 50–200 (green), 200–350 m (red), and 350-bottom (yellow). (d, e) Show the seasonal variability of the cross-shelf transport integrated from Pt100 to Pt200 and from Pt450 to Pt550, respectively. The mean, standard deviation (Std), and standard deviation of the seasonal cycle are indicated.

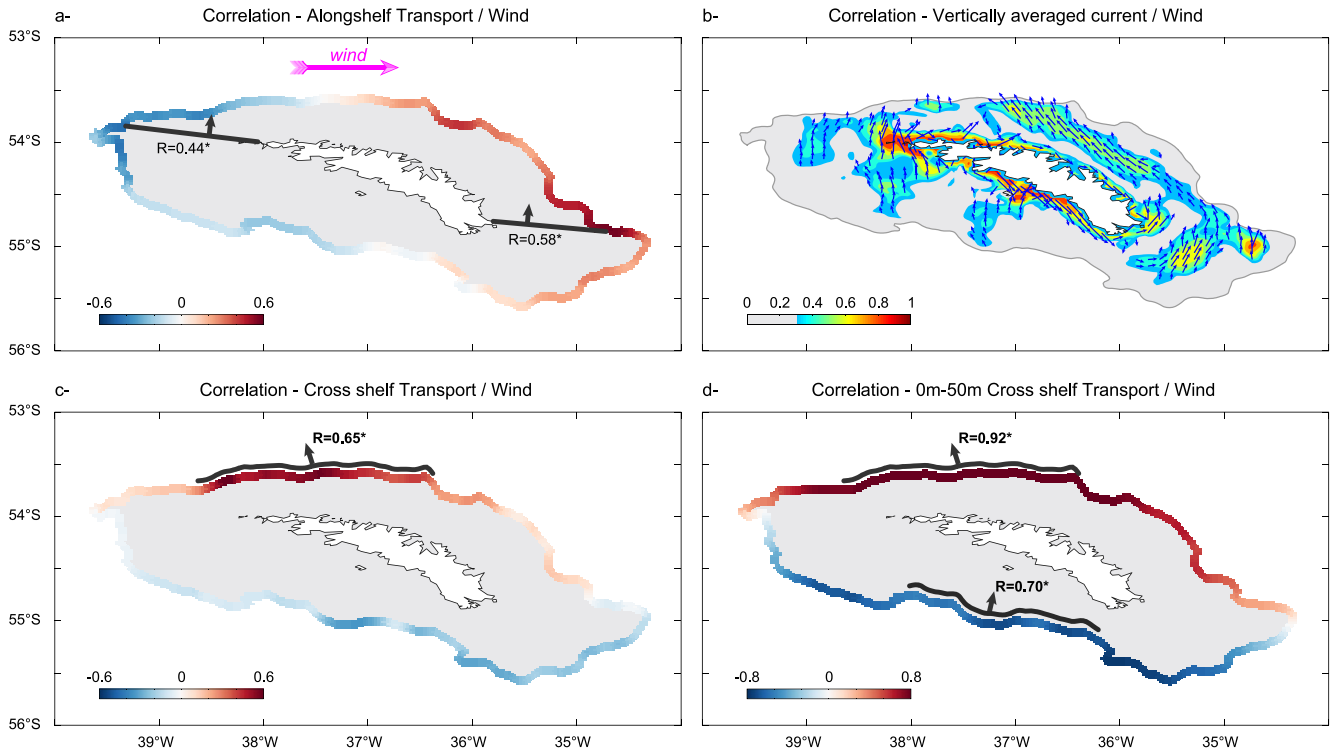

Figure 2. *Wind contribution*. Correlation coefficient between the time series of the zonal wind stress at 37°W–53.5°S and (a) alongshelf transport, (b) vertically averaged shelf current, (c) cross-shelf transport, and (d) cross-shelf transport integrated between surface and 50 m depth. The seasonal variability has been removed in all time series. The gray area corresponds to the shelf region ($H \leq 500$ m).

$R = 0.30$*) northward transport into the canyon south of the SG island. Canyon flows can transport nutrient-rich ACC waters toward the shelf. A detailed analysis of the canyon flows will be presented in a future study using the results of a much higher resolution (1/108°, ~600 m) experiment.

SG is a site of exceptional chlorophyll blooms, which are sustained by the outcropping of nutrient rich waters drawn from the deep layers of the shelf and the open ocean (M20, Borrione et al., 2014; Whitehouse et al., 2008). This outcropping process, which reflects both upwelling and mixing processes, is referred to here as *obduction* (e.g., M20). To characterize the variability of the obduction process we continuously released a passive tracer (TRC_SLP) in a 20 km wide layer surrounding the offshore side of the shelfbreak below 500 m (Figure S1b in Supporting Information S1). Thus, no tracer is released on the top 500 m of the water column. As shown in M20, the main obduction site of this tracer is the northwestern coast of the SG, which is a region of intense wind-driven coastal upwelling (Figure 4a). The time variability of the tracer concentration is very strong; the standard deviation of the surface concentration is of the same order of magnitude as the mean (Figure 4b). A large portion of the tracer variability is associated with seasonal changes of stratification. The non-seasonal variations of tracer concentration show two maxima, one along the northwestern coast of the SG and the other over the outer shelf in the west (Figure 4c). Correlation analysis indicates that these interannual variations are associated with changes in the wind stress forcing in the northern region and with intrusions of the SACCF transport on the western portion of the shelf (Figure 4d).

3.1.3. Variability in Circulation

Seasonal variations of the shelf circulation and the alongshelf transports consist of an intensification of the counterclockwise circulation during summer/fall and a weakening during winter/spring (Figure S3 in Supporting Information S1). The strengthening of the coastal circulation in summer/fall follows changes in the horizontal density gradients. During summer, westerly winds trigger upwelling (downwelling) systems in the northern (southern) portions of the SG coastline. These systems generate strong horizontal density gradients between the coastal region and the mid/outer portions of the shelf (Figure S3c in Supporting Information S1). In winter, the same westerly winds do not produce such intense density horizontal gradient due to well-mixed/unstratified shelf

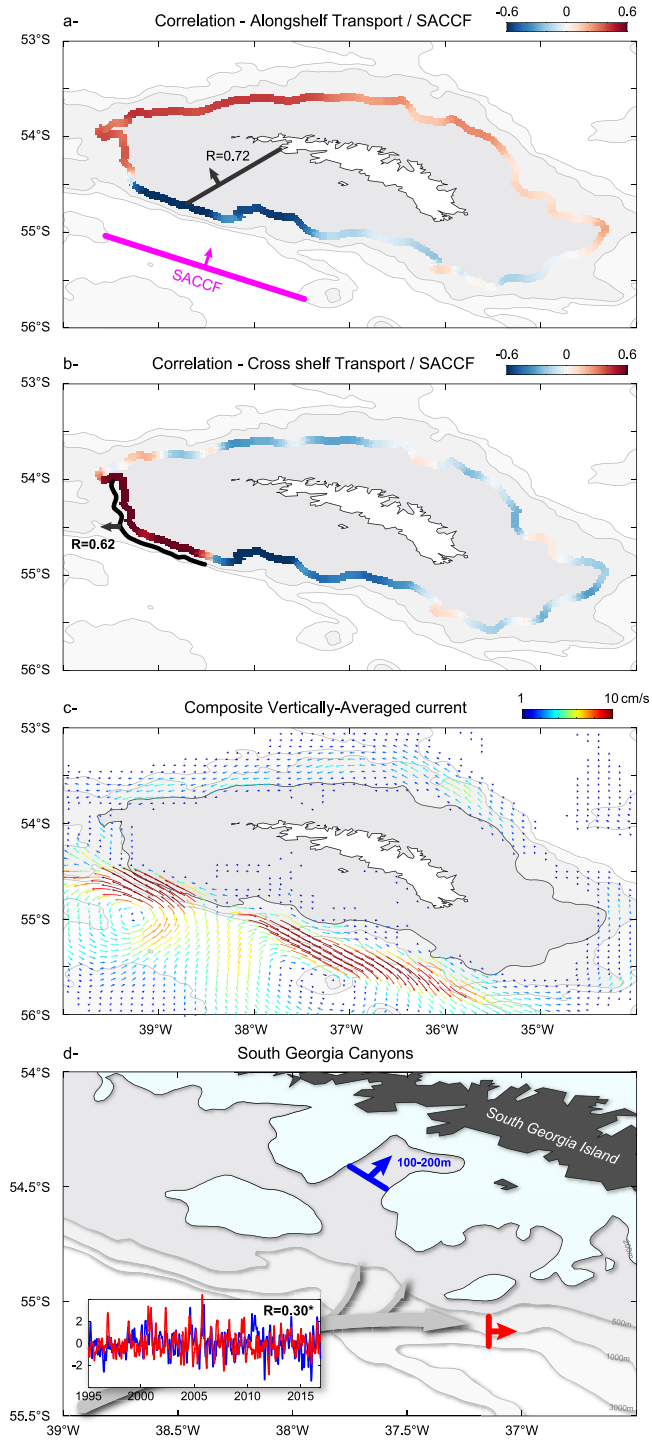

Figure 3. *Southern Antarctic Circumpolar Current Front* (*SACCF*) *contribution*. Correlation coefficient between the time series of the transport across the magenta transect and (a) Alongshelf transport, and (b) cross-shelf transport. (c) Shows the vertically averaged current averaged over the time when the SACCF transport is high (above its standard deviation value). (d) Variability of the SACCF transport computed across the red transect (normalized; red) and variability of the transport into the canyon computed across the blue transect and integrated from 100 to 200 m (normalized; blue). The correlation coefficient between the two time series is $R = 0.30$* and is statistically significant. The seasonal variability has been removed in all time series. The gray areas correspond to the 500 (shelf region), 2,000, and 3,000 m isobaths. Light blue area in panel (d) corresponds to the 200 m isobath.

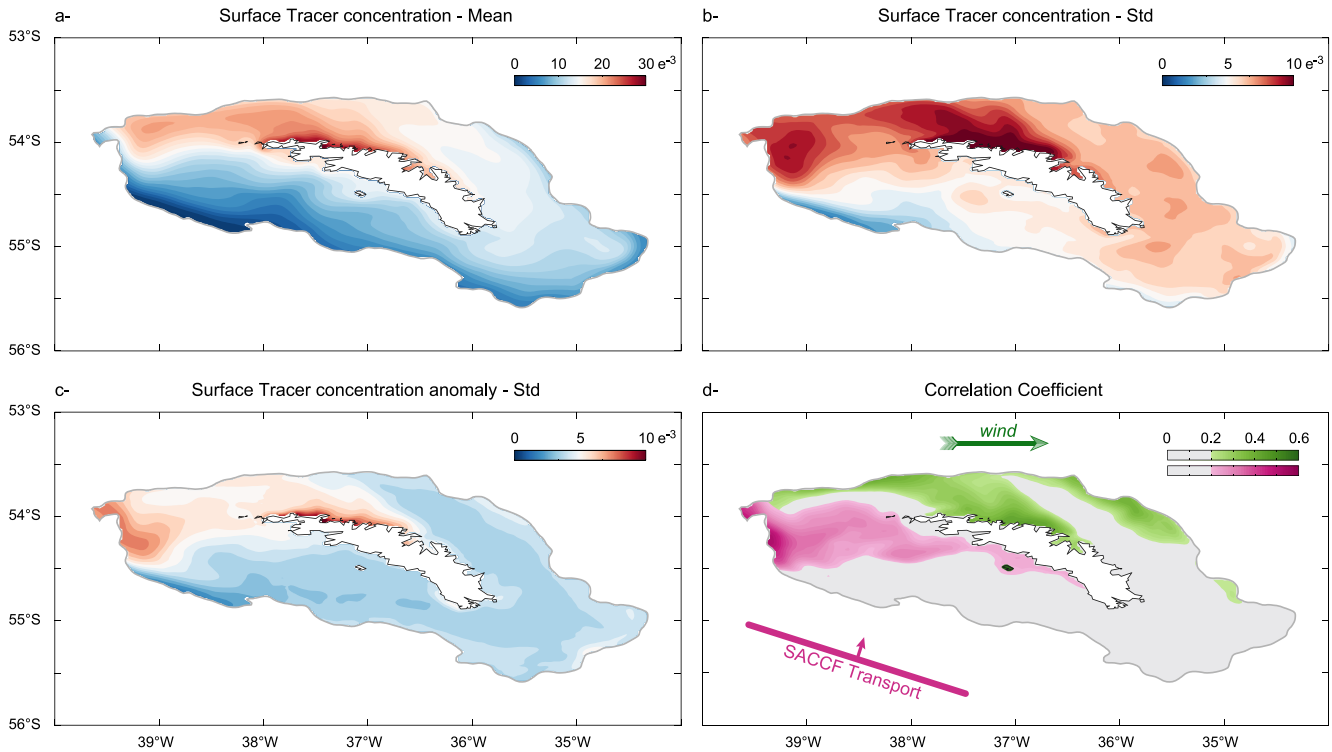

Figure 4. *Obduction/Slope Tracer*. (a) Mean and (b) standard deviation of the Tracer surface concentration. (c) Shows the standard deviation of the Tracer surface concentration after removing its seasonal variability. (d) Correlation coefficient between the surface Tracer concentration and the wind stress at 37°W–53.5°S (green) and correlation coefficient between the surface Tracer concentration and the Southern Antarctic Circumpolar Current Front transport (magenta). The seasonal variability has been removed in all time series in panel (d).

waters. In terms of anomalies, this translates to an intensification of the counterclockwise circulation during summer/fall and a weakening during winter/spring (Figures S3a and S3b in Supporting Information S1). Freshwater inputs from glaciers would also influence (intensify) the horizontal density gradient during summer/fall (Young et al., 2014). Those inputs, however, do not appear to have a significant impact on the seasonal SG circulation. An additional model experiment in which glacial discharges were not included shows that the contribution of these freshwater inputs to the seasonal variability of the circulation is very small or very local. Seasonal variations of the shelf circulation are smaller than interannual variations (illustrated by the standard deviation values on Figure 1b). Cross-shelf exchanges experience also relatively minor seasonal changes ($\sim\pm0.03$ Sv across the shelfbreak in the north and in the south; Figures 1d and 1e). The large standard deviations of the alongshelf transport and cross-shelf exchanges are associated with interannual variations (identified by the standard deviation values on Figures 1b, 1d, and 1e).

To identify the dominant modes of low-frequency variability of SG's circulation we computed the EOFs of surface and vertically averaged currents (Figure 5). The first mode of surface currents shows a predominately zonal flow on the shelf interior, with an intensification of the circulation on the northwestern and southeastern coasts (Figure 5a). This mode explains 38% of the variance and its time series is highly correlated with the zonal winds over the shelf ($R = 0.76$*). Consistent with Ekman dynamics, the correlation coefficient reaches $R = 0.90$* using the southeastward wind component (−40° polar angle). The second mode (not shown, 22% of the variance) consists of a northward shelf flow modulated by the northeastward wind ($R = 0.92$*; 64° polar angle).

The first two modes of the vertically integrated currents reflect the influence of open ocean circulation and wind forcing on SG's circulation. The first mode, which accounts for 18% of the variance, shows an absolute maximum in the southwestern portion of the shelfbreak, which is the region where the SACCF first impacts on SG's shelfbreak (Figure 5b). The time series of this mode is highly correlated with the variability of the SACCF transport ($R = 0.72$*). The first EOF also shows a secondary maximum along a contiguous submarine canyon located in the southwestern region and along the northern portion of the shelfbreak. The second EOF of the

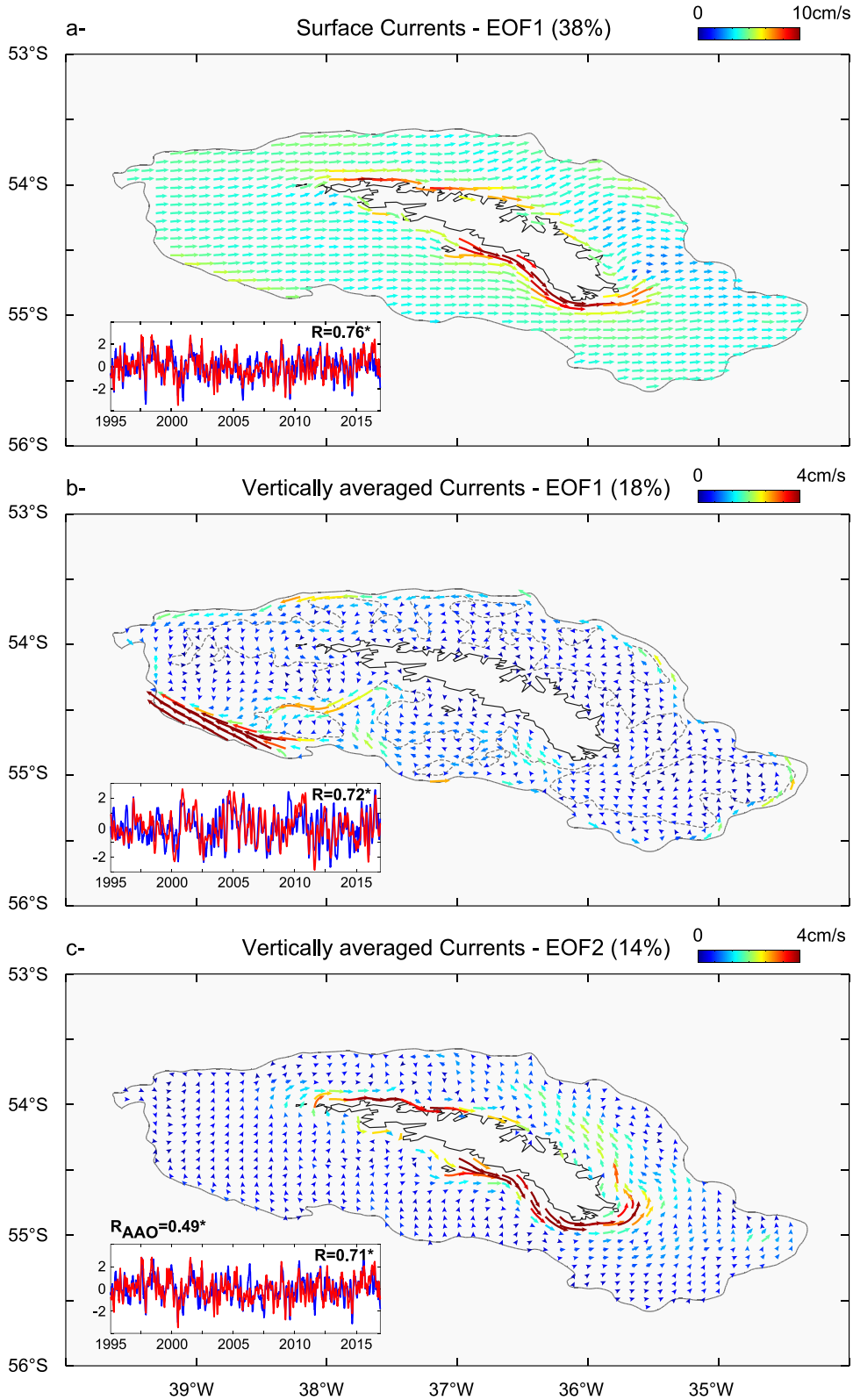

Figure 5.

vertically integrated currents, which explains 14% of the variance, reflects the influence of the wind stress forcing on the shelf circulation (Figure 5c). The time series of this mode is highly correlated with the local zonal winds ($R = 0.71$*; $R = 0.87$* using the southeastward wind component). The amplitude map of the second EOF shows peaks along the coast, which correspond with the upwelling and downwelling coastal jets, and over the mid-shelf jet in the northeastern region. The spatial structure of this mode is similar to the correlation map between wind and vertically averaged currents described previously (Figure 2b). The second mode has a significant correlation with the AAO index ($R = 0.49$*), which represents the changes of the southern Hemisphere high-latitudes winds. This low, yet significant, correlation with the AAO index results from the relatively low correlation between the AAO index and the SG local wind stress ($R = 0.3$, Figure S4a in Supporting Information S1). No correlation is found with the ENSO mode of variability. This is expected since there is no significant correlation between the SOI index and the local wind stress (Figure S4b in Supporting Information S1).

3.2. Sea Surface Temperature Variability

SST variability over the SG region is controlled by local and remote processes, which are modulated on interannual timescales by ENSO and SAM (Meredith et al., 2005, 2008; Trathan & Murphy, 2003; Whitehouse et al., 2008). To characterize the dominant modes of SST variability in our model, we computed the EOFs of its time series. The amplitude of the first EOF mode, which explains 73% of the variance is characterized by a mostly uniform monopole pattern, with a minimum straddling the southern limit of the shelf, which is the region where SACCF waters first encounter the shelf (Figure 6a). Amplitudes and time series of EOF modes computed from observations and the model are quite similar, showing a correlation of $R = 0.78$* (Figure 6b). In our model the dominant SST mode is primarily modulated by the variations of the local heat flux. This conclusion stems from the analysis of an ancillary experiment in which the heat flux only is set to the monthly climatological values. In this experiment—where there are no interannual variations of the heat flux forcing—the correlation between the EOFs of model and observations drops to $R = 0.03$ (from its original value of $R = 0.78$*). The time series of the model's SST mode shows no significant correlation with the local wind ($R = 0.23$), the AAO index ($R = 0.01$), nor with the SACCF transport ($R = 0.01$). Instead, it shows a significant anti-correlation with the SOI at a 4-month lag ($R = -0.49$*, Figure 6c). Warm El Niño conditions over the equatorial Pacific are associated with a cooling of the SG shelf, consistent with in-situ data during the 1997–1998 El Niño event (Meredith et al., 2005). Note that a similar 4-month lag was observed between winter El Niños and an increase of the sea ice extent over the western Antarctic Peninsula (Kim et al., 2016) or the sea ice extent in the Amundsen sea (Yuan & Martinson, 2001).

As shown in prior studies, SST anomalies over the SG shelf are part of a large-scale dipole known as the Antarctic Dipole (Yuan & Martinson, 2000, 2001; Figure S5 in Supporting Information S1). This dipole is a teleconnection pattern linking the edge of the Antarctic sea-ice and the tropical climate variability (Yuan, 2004). During warm El Niño events less/more sea ice is observed in the Pacific/Atlantic sides of the Drake Passage. El Niño warming over the equatorial Pacific strengthens and contracts the Hadley cell in the Pacific and weakens and expands the Hadley cell in the Atlantic shifting the subtropical jet stream toward the equator in the Pacific and toward the poles in the Atlantic (Figure S5b in Supporting Information S1, Yuan, 2004). Simultaneously, the Ferrel cell intensifies and expands in the Pacific and weakens and contracts in the Atlantic triggering an increase of the poleward surface heat flux toward the northern Pacific (warmer SST) and a decrease of the poleward surface heat flux toward the southern Atlantic (colder SST) and thus, toward the SG shelf region (Liu et al., 2002). The opposite occurs during La Niña, when changes in the atmospheric circulation lead to a warming of the SG shelf region. Over the period 1982–2019, the correlation between the monthly SOI index and the first mode of the OSTIA monthly averaged SST anomaly variability over the SG shelf is $R = -0.44$* (Figure S5a in Supporting Information S1). It is known that advective influences also impact the temperatures around South Georgia (Meredith et al., 2008), and, to the extent that shelf-ocean exchange occurs, the shelf waters themselves. Typically, anomalies are created upstream in the ACC by ENSO variations; these take 2–3 years to enter the Atlantic and reach South Georgia (Meredith et al., 2008). The more direct atmospherically driven variations identified here are

Figure 5. *Empirical Orthogonal Function* (*EOFs*). (a) First mode of variability of the surface current (EOF1). The inset panel compares the variability of the EOF1 (blue) and the variability of the zonal wind stress at 37°W–53.5°S (normalized; red). (b, c) Show the first (EOF1) and second (EOF2) modes of variability of the vertically averaged currents, respectively. The inset panel in (b) compares the variability of the EOF1 (blue) and the variability of the Southern Antarctic Circumpolar Current Front transport (normalized; red). The inset panel in (c) compares the variability of the EOF2 (blue) and the variability of the zonal wind stress at 37°W–53.5°S (normalized; red). The correlation coefficient between the EOF2 and the Antarctic Oscillation is 0.47*. The seasonal variability has been removed in all time series. The variance explained by each mode is shown in parenthesis. The gray dashed contour in panel (b) indicates the 200 m isobath.

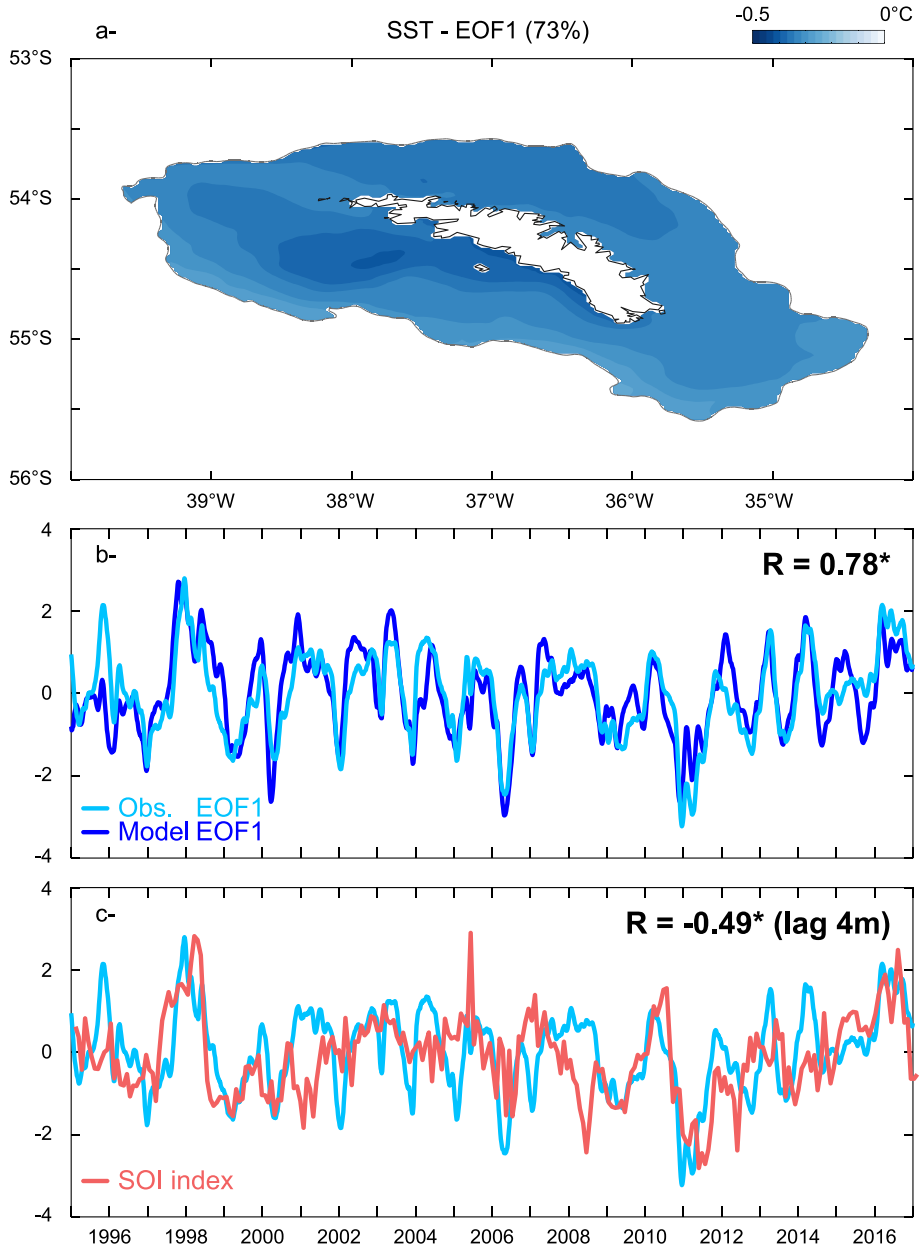

Figure 6. *Sea Surface Temperature* (*SST*) *EOF1*. (a) First mode of the interannual SST variability (EOF1). (b) Compares the variability of the EOF1 computed from the model SST (blue) and from the satellite-derived OSTIA SST (turquoise). The correlation between model and satellite EOF1 SST is 0.78*. The correlation between the monthly satellite SST EOF1 and Southern Oscillation Index index (red) is $R = -0.49$* (c) (lag of 4 months).

overprinted on the advective anomalies, with the typical timescales involved tending to lead to a reinforcement of the signals.

4. Summary

This article characterizes the variability of the SG shelf circulation and cross-shelf transport using the results of a high-resolution (2 km) ocean model for the period 1994–2016. The time mean shelf circulation consists of a counterclockwise gyre with a net onshelf mass flow in the south and net offshelf mass flow in the north. The vertical structure of the cross-shelf exchange is more complex. The cross-shelf flow is in the offshelf direction below 350 m, and in the onshelf direction between 50 and 350 m. In the upper layer the cross-shelf exchange is

consistent with Ekman dynamics of westerly winds with an offshelf transport in the north and an onshelf transport in the south. The seasonal shelf circulation consists of an intensification of the counterclockwise gyre during summer/fall. We find that the seasonal variation is driven by the horizontal density gradients which are set by the westerly winds, seasonal water column stratification, and—to less extent—by the freshwater glaciers' seasonal discharge. In this article, the obduction of deep iron-rich slope water is assessed using modeled passive tracers. On average, the slope water is principally brought to the surface in the north by upwelling favorable winds. Upwelled water variability is at a maximum along the northern coast but is also high over the western outer shelf. A correlation analysis indicates that obduction variability is driven by the local wind stress along the northern coast and is modulated by the SACCF variability in the western shelf.

Winds and the SACCF are the two most important drivers of the SG shelf circulation. To assess the contribution of local and remote forcing on the shelf circulation interannual variability, we identified the dominant modes of low-frequency variability. We find significant correlations between wind stress forcing and the coastal currents, consistent with a geostrophic adjustment from westerly winds. Originating in the SG southern coastal region, the mid-shelf jet located in the northern SG shelf likewise shows significant correlations with the local wind stress. The transport of shelf water to the open-ocean is also significantly correlated with the wind stress variability in the north, in particular in the surface layer. Finally, the largest correlation between the SACCF and the shelf circulation variability is observed in the southwestern shelf where the SACCF encounters the SG shelf slope.

An EOF decomposition of the shelf circulation interannual variability indicates that the first mode of variability is highly correlated with the SACCF variability, while the second mode is modulated by the local wind stress. The second mode shows significant correlation with the AAO large scale climate index, which represents the change of magnitude of the zonal wind stress over the Southern Ocean. We do not find a significant correlation with the El Niño Southern Oscillation and the shelf circulation variability. ENSO is however significantly correlated with the shelf SST interannual variability, such that warm El Niño conditions over the equatorial Pacific are associated with a cooling of the SG shelf.

This study provides a dynamical framework to interpret and predict how the SG circulation has and will respond to large scale climate forcing. Understanding the shelf circulation variability (and the processes driving it) is a key step to improving predictive skill. In particular, it is known that the winds have strengthened in recent decades and are expected to continue. Model simulations from the Coupled Model Intercomparison Project latest Phase 6 indicate that the Southern Hemisphere westerly winds will continue to strengthen and move poleward over the next century under most climate change scenarios (Deng et al., 2022). Such atmospheric changes will have a direct effect on the coastal upwelling and the export of nutrients to the open-ocean, required to sustain the SG bloom. Potential future changes in the SACCF transport will also matter for the obduction of macro-nutrient and iron rich Circumpolar Deep Water onto the shelf.

Acknowledgments
The authors thank the two anonymous reviewers for their insightful comments and suggestions. V. Combes and R. Matano acknowledge the support of NSF Grants OCE-1830856, OCE-2149093, and OCE-2149292 and NASA Award 80NSSC21K0559. V. Combes also acknowledges the support from the Ramón y Cajal Program (RYC2020-029306-I) and from the European Social Fund/Universitat de les Illes Balears/Spanish State Research Agency (AEI—10.13039/501100011033). The present research was carried out within the framework of the activities of the Spanish Government through the "Maria de Maeztu Centre of Excellence" accreditation to IMEDEA (CSIC-UIB) (CEX2021-001198). The participation of M. Meredith and E. Young was funded by the Natural Environment Research Council via the BAS Polar Oceans program, including Award NE/W004933/1 (BIOPOLE).

Data Availability Statement

The ROMS/AGRIF model used in this study can be downloaded from https://www.croco-ocean.org/download/roms_agrif-project/. ERA5 atmospheric reanalysis data were downloaded from https://cds.climate.copernicus.eu/cdsapp#!/dataset/reanalysis-era5-single-levels?tab=form. QSCAT and ASCAT scatterometer data can be downloaded from https://cersat.ifremer.fr/Data/Catalogue. Tidal TPXO9 data can be obtained from https://www.tpxo.net/global/tpxo9-atlas. Bottom topography data can be obtained from https://www.gebco.net/. The model vertically averaged velocity, surface velocity, sea surface temperature, surface Tracer TRC_SLP concentration, SACCF transport, and wind stress time series used in this study are deposited in the Harvard Dataverse (Combes, 2023). The 3D fields are available upon request.

References

Borrione, I., Aumont, O., Nielsdóttir, M. C., & Schlitzer, R. (2014). Sedimentary and atmospheric sources of iron around South Georgia, Southern Ocean: A modelling perspective. *Biogeosciences*, *11*(7), 1981–2001. https://doi.org/10.5194/bg-11-1981-2014

Cai, W. J., Whetton, P. H., & Karoly, D. J. (2003). The response of the Antarctic Oscillation to increasing and stabilized atmospheric CO_2. *Journal of Climate*, *16*(10), 1525–1538. https://doi.org/10.1175/1520-0442-16.10.1525

Combes, V. (2023). Replication data for: Variability of the shelf circulation Around South Georgia, Southern Ocean [Dataset]. Harvard Dataverse, V1. https://doi.org/10.7910/DVN/76UHAK

Combes, V., & Matano, R. P. (2014). A two-way nested simulation of the oceanic circulation in the Southwestern Atlantic. *Journal of Geophysical Research: Oceans*, *119*(2), 731–756. https://doi.org/10.1002/2013JC009498

Deacon, G. E. R. (1977). *Seasonal and annual variations in water temperature and salinity near South Georgia, 1925–1937*. Report No 49 (p. 29). Institute of Oceanographic Sciences.

Debreu, L., Marchesiello, P., Penven, P., & Cambon, G. (2011). Two-way nesting in split-explicit ocean models: Algorithms, implementation and validation. *Ocean Modelling*, *49*(50), 1–21. https://doi.org/10.1016/j.ocemod.2012.03.003

Deng, K., Azorin-Molina, C., Yang, S., Hu, C., Zhang, G., Minola, L., & Chen, D. (2022). Changes of Southern Hemisphere westerlies in the future warming climate. *Atmospheric Research*, *270*, 106040. https://doi.org/10.1016/j.atmosres.2022.106040

Egbert, G. D., & Erofeeva, S. Y. (2002). Efficient inverse modeling of barotropic ocean tides. *Journal of Atmospheric and Oceanic Technology*, *19*(2), 183–204. https://doi.org/10.1175/1520-0426(2002)019<0183:eimobo>2.0.co;2

Fielding, S., Watkins, J. L., Trathan, P. N., Enderlein, P., Waluda, C. M., Stowasser, G., et al. (2014). Interannual variability in Antarctic krill (Euphausia superba) density at South Georgia, Southern Ocean: 1997–2013. *ICES Journal of Marine Science*, *71*(9), 2578–2588. https://doi.org/10.1093/icesjms/fsu104

Fyfe, J. C., Boer, G. J., & Flato, G. M. (1999). The Arctic and Antarctic Oscillations and their protected changes under global warming. *Geophysical Research Letters*, *26*(11), 1601–1604. https://doi.org/10.1029/1999gl900317

Good, S., Fiedler, E., Mao, C., Martin, M. J., Maycock, A., Reid, R., et al. (2020). The current configuration of the OSTIA system for operational production of foundation sea surface temperature and ice concentration analyses. *Remote Sensing*, *12*(4), 720. https://doi.org/10.3390/rs12040720

Hao, X., He, S. P., Wang, H. J., & Han, T. T. (2017). The impact of long-term oceanic warming on the Antarctic Oscillation in austral winter. *Scientific Reports*, *7*(1), 12321. https://doi.org/10.1038/s41598-017-12517-x

Hardy, A. C., & Gunther, E. R. (1935). The plankton of the South Georgia whaling grounds and adjacent waters, 1926–27. *Discovery Reports*, *11*, 1–456.

Hart, T. J. (1934). The plankton of the southwest Atlantic and the Bellingshausen Sea 1929–1931. *Discovery Reports*, *8*, 1–268.

Hersbach, H., Bell, B., Berrisford, P., Biavati, G., Horányi, A., Muñoz Sabater, J., et al. (2018). ERA5 hourly data on single levels from 1979 to present. *Copernicus Climate Change Service (C3S) Climate Data Store (CDS)*. https://doi.org/10.24381/cds.adbb2d47

Kim, H., Doney, S. C., Iannuzzi, R. A., Meredith, M. P., Martinson, D. G., & Ducklow, H. W. (2016). Climate forcing for dynamics of dissolved inorganic nutrients at Palmer Station, Antarctica: An interdecadal (1993–2013) analysis. *Journal of Geophysical Research: Biogeosciences*, *121*(9), 2369–2389. https://doi.org/10.1002/2015JG003311

Liu, J., Yuan, X., Rind, D., & Martinson, D. G. (2002). Mechanism study of the ENSO and southern high latitude climate teleconnections. *Geophysical Research Letters*, *29*(14), 24-1–24-4. https://doi.org/10.1029/2002GL015143

Maslennikov, V. V., & Solyankin, Y. V. (1981). Interannual displacements of the zone of interaction of Weddell Sea waters with the Antarctic circumpolar current. *Polar Geography*, *5*(1), 45–50. https://doi.org/10.1080/10889378109388672

Matano, R. P., Combes, V., Young, E. F., & Meredith, M. (2020). Modeling the impact of ocean circulation on chlorophyll blooms Around South Georgia, Southern Ocean. *Journal of Geophysical Research: Oceans*, *125*(9), e2020JC016391. https://doi.org/10.1029/2020JC016391

Matano, R. P., & Palma, E. D. (2008). On the upwelling of downwelling currents. *Journal of Physical Oceanography*, *38*(11), 2482–2500. https://doi.org/10.1175/2008jpo3783.1

Meredith, M. P., Murphy, E. J., Brandon, M. A., Trathan, P. N., Thorpe, S. E., Bone, D. G., et al. (2005). Variability of hydrographic conditions to the east and northwest of South Georgia, 1996–2001. *Journal of Marine Systems*, *53*(1–4), 143–167. https://doi.org/10.1016/j.jmarsys.2004.05.005

Meredith, M. P., Murphy, E. J., Hawker, E. J., King, J. C., & Wallace, M. I. (2008). On the interannual variability of ocean temperatures around South Georgia, Southern Ocean: Forcing by El Niño/Southern Oscillation and the Southern annular mode. *Deep-Sea Research Part II*, *55*(18–19), 2007–2022. https://doi.org/10.1016/j.dsr2.2008.05.020

Meredith, M. P., Watkins, J. L., Murphy, E. J., Ward, P., Bone, D. G., Thorpe, S. E., & Ladkin, R. S. (2003). Southern ACC front to the northeast of South Georgia: Pathways, characteristics, and fluxes. *Journal of Geophysical Research*, *108*(C5), 3162. https://doi.org/10.1029/2001jc001227

Miller, R. N., Matano, R. P., & Palma, E. D. (2011). Shelfbreak upwelling induced by alongshore currents: Analytical and numerical results. *Journal of Fluid Mechanics*, *686*, 239–249. https://doi.org/10.1017/jfm.2011.326

Shchepetkin, A. F., & McWilliams, J. C. (2005). The regional oceanic modeling system (ROMS): A split-explicit, free-surface, topography-following-coordinate oceanic model. *Ocean Modelling*, *9*(4), 347–404. https://doi.org/10.1016/j.ocemod.2004.08.002

Shindell, D. T., & Schmidt, G. A. (2004). Southern Hemisphere climate response to ozone changes and greenhouse gas increases. *Geophysical Research Letters*, *31*(18), L18209. https://doi.org/10.1029/2004GL020724

Thorpe, S. E., Heywood, K. J., Brandon, M. A., & Stevens, D. P. (2002). Variability of the southern Antarctic circumpolar current front north of South Georgia. *Journal of Marine Systems*, *37*(1–3), 87–105. https://doi.org/10.1016/s0924-7963(02)00197-5

Thorpe, S. E., Heywood, K. J., Stevens, D. P., & Brandon, M. A. (2004). Tracking passive drifters in a high resolution ocean model: Implications for interannual variability of larval krill transport to South Georgia. *Deep Sea Research Part I: Oceanographic Research Papers*, *51*(7), 909–920. https://doi.org/10.1016/s0967-0637(04)00034-2

Trathan, P. N., Brandon, M. A., & Murphy, E. J. (1997). Characterization of the Antarctic polar frontal zone to the north of South Georgia in summer 1994. *Journal of Geophysical Research*, *102*(C5), 10483–10497. https://doi.org/10.1029/97jc00381

Trathan, P. N., Brandon, M. A., Murphy, E. J., & Thorpe, S. E. (2000). Transport and structure within the Antarctic circumpolar current to the north of South Georgia. *Geophysical Research Letters*, *27*(12), 1727–1730. https://doi.org/10.1029/1999gl011131

Trathan, P. N., Brierley, A. S., Brandon, M. A., Bone, D. G., Goss, C., Grant, S. A., et al. (2003). Oceanographic variability and changes in Antarctic krill (Euphausia superba) abundance at South Georgia. *Fisheries Oceanography*, *12*(6), 569–583. https://doi.org/10.1046/j.1365-2419.2003.00268.x

Trathan, P. N., & Murphy, E. J. (2003). Sea surface temperature anomalies near South Georgia: Relationships with the Pacific ElNiño regions. *Journal of Geophysical Research*, *107*(C4), 8075. https://doi.org/10.1029/2000JC000299

Whitehouse, M. J., Korb, R. E., Atkinson, A., Thorpe, S. E., & Gordon, M. (2008). Formation, transport and decay of an intense phytoplankton bloom within the high-nutrient low-chlorophyll belt of the Southern Ocean. *Journal of Marine Systems*, *70*(1–2), 150–167. https://doi.org/10.1016/j.jmarsys.2007.05.003

Whitehouse, M. J., Priddle, J., & Symon, C. (1996). Seasonal and annual change in seawater temperature, salinity, nutrient and chlorophyll a distributions around South Georgia, South Atlantic. *Deep Sea Research Part I: Oceanographic Research Papers*, *43*(4), 425–443. https://doi.org/10.1016/0967-0637(96)00020-9

Young, E. F., Meredith, M. P., Murphy, E. J., & Carvalho, G. R. (2011). High-resolution modeling of the shelf and open ocean adjacent to South Georgia, Southern Ocean. *Deep Sea Research Part II: Topical Studies in Oceanography*, *58*(13–16), 1540–1552. https://doi.org/10.1016/j.dsr2.2009.11.003

Young, E. F., Thorpe, S. E., Banglawala, N., & Murphy, E. J. (2014). Variability in transport pathways on and around the South Georgia shelf, Southern Ocean: Implications for recruitment and retention. *Journal of Geophysical Research: Oceans*, *119*(1), 241–252. https://doi.org/10.1002/2013JC009348

Yuan, X. (2004). ENSO-Related impacts on Antarctic sea ice: A synthesis of phenomenon and mechanisms. *Antarctic Science*, *16*(4), 415–425. https://doi.org/10.1017/S0954102004002238

Yuan, X., & Martinson, D. G. (2000). Antarctic sea ice variability and its global connectivity. *Journal of Climate*, *13*(10), 1697–1717. https://doi.org/10.1175/1520-0442(2000)013<1697:asieva>2.0.co;2

Yuan, X., & Martinson, D. G. (2001). The Antarctic dipole and its predictability. *Geophysical Research Letters*, 28(18), 3609–3612. https://doi.org/10.1029/2001gl012969